Transition Metal Chemistry (2020) 45:363–372
https://doi.org/10.1007/s11243-020-00388-7

Structurally characterized dinuclear zinc(II) and copper(II) coumarin-based N_2O_2-donor complexes: syntheses, Hirshfeld analyses and fluorescent properties

Wen-Jing She[1] · Yong-Fan Cui[2] · Chang Liu[2] · Li Wang[2]

Received: 2 March 2020 / Accepted: 3 April 2020 / Published online: 22 April 2020

Abstract
Two newly designed dinuclear Zn^{II} and Co^{II} complexes $[Co_2(L)_2]\cdot H_2O$ (**1**) and $[Zn_2(L)_2]\cdot H_2O$ (**2**) of a coumarin-based N_2O_2-donor ligand H_2L (5′-(*N*,*N*′-diethylamino)-6′-methyl-2,2′-[ethylenedioxybis(nitrilomethylidyne)]phenolcoumarinphenol) were synthesized and characterized by physicochemical and spectroscopic methods. Complexes **1** and **2** are extremely rare asymmetric binuclear structures. The structures of complexes **1** and **2** are isostructural. In both complexes, one metal atom (Co2 or Zn1) adopts a twisted square pyramid configuration, while another metal atom (Co1 or Zn2) adopts a twisted triangular bipyramid configuration with penta-coordination. In addition, complexes **1** and **2** form 3D supramolecular structures through intermolecular hydrogen bonding interactions. Furthermore, the Hirshfeld surfaces analyses and fluorescence properties of complexes **1** and **2** have been discussed in detail.

Introduction

Salen-like complexes have been continuously developed in different fields due to their special three-dimensional structures and unique electronic structures [1–5]. Later, the salamo-like ligands with a N_2O_2 coordination environment were obtained by modifying the salen-like ligands, which have the advantage of introducing more negatively charged oxygen atoms into the diamine to enhance its stability. Therefore, salamo-like complexes have enriched the types of complexes in structure, have been greatly supplemented in the field of supramolecular chemistry and have played an indispensable role in the field of coordination chemistry [6–11]. These metal complexes are used as catalysts [12], magnetic materials [13–17], nonlinear optical materials [18–20], luminescence materials [21–30], molecular identifiers [31–33], supramolecular architectures [34–37], dye and pigments [38], have application in biological fields [3] among other applications, and have great future prospects. In recent years, through the study of the fluorescent properties of metal complexes with different structures, it has been found that for many metal complexes, the interaction between the metal ions and the ligands changes the electronic excited state of the metal center, so that these metal complexes show many interesting fluorescent properties [39–42].

In this paper, two new dinuclear Co^{II} and Zn^{II} complexes were synthesized by the reactions of H_2L with $Co(OAc)_2\cdot 4H_2O$ and $Zn(OAc)_2\cdot 2H_2O$, respectively; the Hirshfeld surfaces analyses and fluorescence properties of complexes **1** and **2** were investigated.

Experimental

Materials and methods

4-(*N*,*N*′-Diethylamino)salicylicaldehyde (99%) and 7-hydroxy-4-methylcoumarin (98%) were purchased from Alfa Aesar (New York, NY, USA) and used without further purification. All other reagents and chemicals are from Tianjin Chemical Reagent Factory. The melting points

Electronic supplementary material The online version of this article (https://doi.org/10.1007/s11243-020-00388-7) contains supplementary material, which is available to authorized users.

✉ Li Wang
wangli_78@126.com

[1] College of Art and Design, Lanzhou Jiaotong University, Lanzhou 730070, People's Republic of China

[2] School of Chemical and Biological Engineering, Lanzhou Jiaotong University, Lanzhou 730070, People's Republic of China

were measured via an X_4 microscopic melting point meter from Beijing Taike Instrument Co., Ltd. Carbon, hydrogen and nitrogen elemental analysis data are obtained from the GmbH VarioEL V3.00 automatic elemental analyzer. Elemental analysis of Co^{II} and Zn^{II} was detected by IRIS ER/S-WP-1 ICP atomic emission spectrometer (Berlin, Germany). UV/Vis spectra were measured by a Shimadzu UV-2550 spectrometer (Hitachi, Tokyo, Japan). The fluorescence spectra were measured on an F-7000 FL spectrophotometer (Hitachi, Tokyo, Japan). The infrared spectra were measured with a VERTEX-70 FT-IR spectrophotometer (Bruker, Germany), and the sample was prepared as KBr (500–4000 cm^{-1}). The single-crystal X-ray structures were determined on a Bruker APEX-II CCD diffractometer.

Preparation of H_2L

H_2L was prepared according to similar method previously reported [43]. 1,2-Bis(aminooxy)ethane and 8-formyl-7-hydroxy-4-methylcoumarin were prepared according to previous literature [44, 45].

4-(*N*,*N*'-diethylamino)-2-[*O*-(1-ethyloxyamide)]oximephenol: 4-(*N*, *N*'-diethylamino) salicylicaldehyde (385.6 mg, 2.00 mmol) was dissolved in a methanol solution (25 mL) and slowly added to a methanol solution (50 mL) of 1,2-bis(aminooxy)ethane (184.3 mg, 2.00 mmol) for 4 h. The above solution was heated at 55 °C for about 5 h. After cooling to room temperature, the red-brown oil obtained by distillation under reduced pressure was separated by column chromatography using ethyl acetate/chloroform (1:20, V/V), and 78.5 mg white solid 4-(*N*,*N*'-diethylamino)-2-[*O*-(1-ethyloxyamide)]oximephenol was gained by distillation under reduced pressure.

H_2L: a above-obtained 4-(*N*,*N*'-diethylamino)-2-[*O*-(1-ethyloxyamide)]oximephenol (262.21 mg, 1.00 mmol) in ethanol (25 mL) was added to a solution of 4-methyl-7-hydroxy-8-formylcoumarin (204.17 mg, 1.00 mmol) in ethanol (30 mL). The mixed solution was heated to ca. 80 °C and refluxed for 4–5 h. The solution was cooled to room temperature to obtain a white precipitate H_2L, filtered and dried, as given in Scheme 1. Yield 51.7%. m.p.148–149 °C. Anal. Calcd. for $C_{24}H_{27}N_3O_6$ (%): C, 63.56; H, 6.00; N, 9.27. Found: C, 63.72; H, 5.89; N, 9.08.

Preparation of complex 1

A solution of $Co(OAc)_2{\cdot}4H_2O$ (2.50 mg, 0.01 mmol) in ethanol (5 mL) was added to a solution of H_2L (4.53 mg, 0.01 mmol) in acetone (5 mL) at room temperature. The color of the mixture turned to red-brown immediately, and then, the mixture was stirred at room temperature for about 30 min. The mixture was filtered off, and the filtrate was allowed to stand at room temperature for about 1 week. The solvent was partially evaporated, and a transparent red block single crystal suitable for X-ray crystallographic analysis was obtained. Anal. Calcd. for $C_{48}H_{52}Co_2N_6O_{13}$ (1038.84) (%): C, 55.50; H, 5.05; N, 8.09; Co, 11.35. Found: C, 51.72; H, 5.01; N, 7.95; Co, 11.12.

Preparation of complex 2

A solution of $Zn(OAc)_2{\cdot}2H_2O$ (2.20 mg, 0.01 mmol) in ethanol (5 mL) was added to a solution of H_2L (4.53 mg, 0.01 mmol) in dichloromethane (5 mL) at room temperature. The mixture is colorless, and then, the mixture was stirred at room temperature for about 30 min. The mixture was filtered off, and the filtrate was allowed to stand at room temperature for about 1 week. The solvent was partially evaporated, and a transparent colorless needle-like single crystal suitable for X-ray crystallographic analysis was obtained. Anal. Calcd. for $C_{48}H_{52}Zn_2N_6O_{13}$ (1051.73) (%): C, 54.82; H, 4.98; N, 7.99; Zn, 12.43. Found: C, 54.98; H, 5.02; N, 7.84; Zn, 12.27.

Crystal structure determinations of complexes 1 and 2

X-ray diffraction data of complexes **1** and **2** were collected at 100.01(10) K, use a BRUKER SMART APEX-II CCD diffractometer with graphite monochromated Cu-K*a* and Mo–K*a* radiations ($\lambda = 1.54178$ Å and $\lambda = 0.71073$ Å), respectively. The LP factor and semiempirical absorption corrections were applied to the intensity data. Then, the structures were solved using SHELXS-1997 [46] and by a full matrix least-squares technique based on F^2 using SHELXL-2014 and SHELXL-2015 [47]. The anisotropic thermal parameters are assigned to all non-hydrogen atoms.

Scheme 1 Synthetic route to H_2L

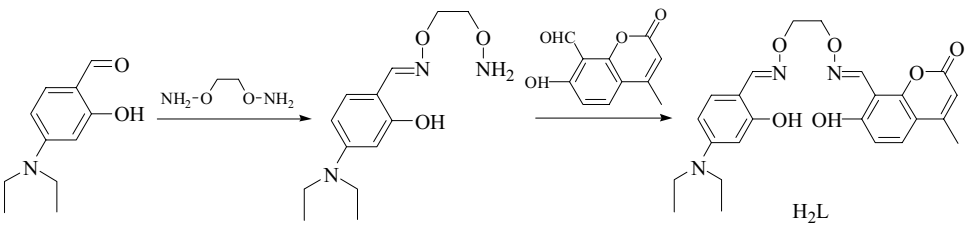

Contributions to scattering due to these highly disordered solvent molecules were removed using the SQUEEZE routine of PLATON; the structures were then refined again using the data generated. Crystal data and experimental parameters relevant to the structure determinations with respect to complexes **1** and **2** are listed in Table 1.

Results and discussion

Salamo-like complexes **1** and **2** have been appropriately prepared and characterized by IR, UV–Vis and fluorescence spectroscopy, X-ray crystallography and Hirshfeld surfaces analyses.

FT-IR spectra

Infrared spectra of H_2L and its complexes **1** and **2** exhibited different bands in 4000–500 cm^{-1} region (Table 2). The IR spectral details of H_2L and its complexes **1** and **2** are given in Fig. 1. The O–H stretching band of H_2L is found at ca. 3417 cm^{-1} that belongs to the phenolic hydroxyl groups [8]. However, these bands are not

Table 2 The major FT-IR spectra of H_2L and its complexes **1** and **2** (cm^{-1})

Complexes	$\nu_{(O–H)}$	$\nu_{(C=N)}$	$\nu_{(Ar–O)}$	$\nu_{(C=O)}$	$\nu_{(M–O)}$
H_2L	3417	1634	1292	1728	–
1	–	1617	1242	1733	520
2	–	1621	1241	1735	513

Table 1 Crystal data and structure refinement parameters for **1** and **2**

Coordination compound	**1**	**2**
Formula	$C_{48}H_{52}Co_2N_6O_{13}$	$C_{48}H_{52}Zn_2N_6O_{13}$
Formula weight	1038.81	1051.69
Temperature (K)	100.01(10)	100.00(10)
Wavelength (Å)	1.54178	0.71073
Crystal system	Orthorhombic	Orthorhombic
Space group	P_{bca}	P_{bca}
Unit cell dimensions		
a (Å)	17.8736(5)	17.8697(6)
b (Å)	14.7661(4)	14.8133(5)
c (Å)	36.3681(14)	36.2496(13)
α (°)	90	90
β (°)	90	90
γ (°)	90	90
V (Å^3)	9598.4(5)	9595.6(6)
Z	8	8
D_c (g cm^{-3})	1.438	1.456
μ (mm^{-1})	6.013	1.071
F (000)	4320	4368
Crystal size (mm)	0.14×0.12×0.11	0.12×0.11×0.1
θ range (°)	2.430–66.498	2.110–26.500
Index ranges	$-21 \le h \le 20$ $-17 \le k \le 17$ $-43 \le l \le 41$	$-17 \le h \le 22$ $-14 \le k \le 18$ $-45 \le l \le 42$
Reflections collected	25,071	31,134
Independent reflections	8455	9920
R_{int}	0.0587	0.0492
Completeness (%)	99.9	99.8
Data/restraints/parameters	8455/19/649	9920/49/651
GOF	1.047	1.131
Final R_1, wR_2 indices [$I > 2\sigma(I)$]	0.0670/0.1641	0.0625/0.1294
R_1, wR_2 indices (all data)	0.1075/0.1891	0.0921/0.1422
Largest differences peak and hole (e Å^{-3})	0.957/−0.658	0.880/−0.695

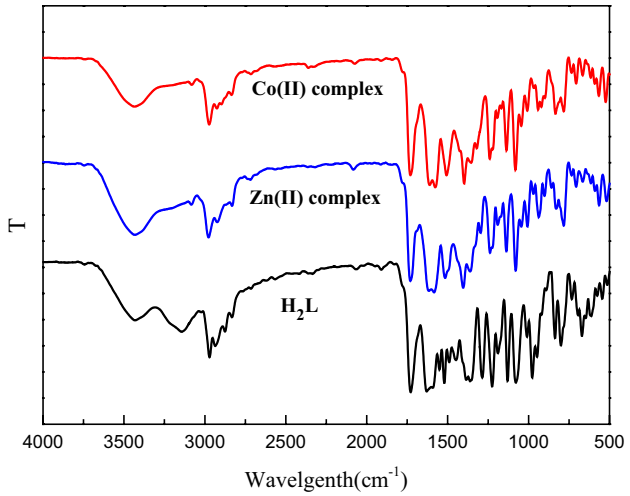

Fig. 1 The IR spectra of H_2L and its complexes **1** and **2**

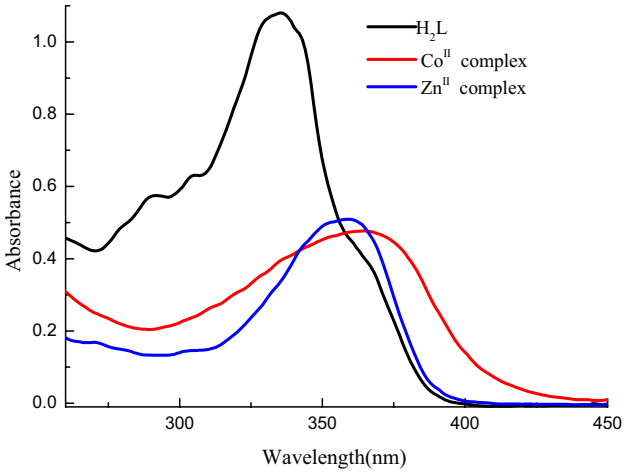

Fig. 2 UV–Vis spectra of H_2L and its complexes **1** and **2**

observed in complexes **1** and **2**, indicating that the phenolic O–H groups of H_2L are fully deprotonated. New O–H stretching vibration bands in complexes **1** and **2** are observed at around 3437 and 3442 cm^{-1} corresponding to crystallizing water molecules [26]. The C=N stretching vibration band of H_2L is observed at ca. 1634 cm^{-1}, while those of complexes **1** and **2** are found at ca. 1617 and 1621 cm^{-1}. The typical C=N stretching frequencies are moved to lower frequencies, showing that the Co^{II} and Zn^{II} atoms are coordinated to the oxime nitrogen atoms [9]. The typical Ar–O stretching band of H_2L emerges at approximately 1292 cm^{-1}, and after coordination, the stretching bands of complexes **1** and **2** shift to low wave numbers, at approximately 1242 and 1241 cm^{-1}, showing that the Co–O and Zn–O coordinate bonds have been formed [10]. In addition, the stronger absorption band of H_2L at 1728 cm^{-1} is attributed to the stretching vibration of the C=O double bond of coumarin; the C=O stretching vibration of complexes **1** and **2** compared to H_2L appears at about 1733 and 1735 cm^{-1} and is attributed to the formation of M–N/O after coordination between H_2L and the metal. New moderate intensity M–O vibrational bands in complexes **1** and **2** appear at 520 and 513 cm^{-1} [48, 49].

UV–Vis spectra

UV–Vis spectra of the free ligand H_2L and its complexes **1** and **2** in 2.5×10^{-5} mol/L^{-1} ethanol solution are shown in Fig. 2.

The absorption spectra of H_2L and its complexes **1** and **2** are given in Fig. 2. In the UV–Vis absorption spectrum of the free ligand H_2L, absorption peaks appear at approximately 291, 336 and 368 nm, respectively. The absorption peak at 289 nm is attributed to the π–π* transition of the benzene ring, the second peak at 336 nm could be assigned to the n–π* transition of the C=N bond in the ligand, and the last absorption peak at 368 nm is assigned to the π–π* transition to the carbonyl group in coumarin. Compared with the free ligand H_2L, complexes **1** and **2** have obvious absorption peaks at approximately 360 and 366 nm, which are assigned to L → M charge-transfer (LMCT) transitions [50].

Descriptions of the crystal structures

Selected bond lengths and angles are listed separately in Table 3. The corresponding hydrogen bonding interactions of complexes **1** and **2** are summarized in Table 4.

For complexes **1** and **2**, all M^{II} atoms are located at the N_2O_2 site of the deprotonated ligand $(L)^{2-}$ moiety with two atoms (O6 and O12) from the other salamo-type ligand $(L)^{2-}$ moiety, and the two M^{II} atoms are connected in a M–O–M fashion through phenol oxygen atoms, and the crystal structures feature two-fold symmetry. At the same time, the two M^{II} atoms of complexes **1** and **2** are pentacoordinated and adopt slightly twisted trigonal bipyramidal geometries (Co1 and Zn2) and square pyramid configuration (Co2 and Zn1) geometries (Figs. 3b and 5b) [44], which are deduced by calculating the values of $\tau_{Co1}=0.57$, $\tau_{Co2}=0.45$, $\tau_{Zn1}=0.45$ and $\tau_{Zn2}=0.59$, respectively [46]. From the calculation results, it can be seen that the τ values of Co1 and Zn2 are both greater than 0.5, forming trigonal bipyramidal geometries, and the τ values of Co2 and Zn1 are less than 0.5, forming square pyramid configurations. X-ray crystal structure measurement shows that complexes **1** and **2** are asymmetric binuclear structures and crystallize in the orthorhombic system, space group *P*bca. The structure consists of two M^{II} atoms (M1 and M2), two completely deprotonated $(L)^{2-}$ units, and one lattice water molecule, and forms an extremely rare 2:2 (molar ratio of L^{2-}:M^{II} atom)

Table 3 Selected bond lengths (Å) and angles (°) for **1** and **2**

1			
Bond	Lengths	Bond	Lengths
Co1–O3	1.927(3)	Co2–O6	1.998(3)
Co1–O6	2.114(3)	Co2–O9	1.933(3)
Co1–O12	2.011(3)	Co2–O12	2.074(3)
Co1–N1	2.084(4)	Co2–N4	2.063(4)
Co1–N2	2.014(4)	Co2–N5	2.032(4)
Bond	Angles	Bond	Angles
O3–Co1–O6	106.35(13)	O6–Co2–O9	113.43(13)
O3–Co1–O12	112.55(13)	O6–Co2–O12	78.49(13)
O3–Co1–N1	89.10(15)	O6–Co2–N4	98.08(14)
O3–Co1–N2	116.81(15)	O6–Co2–N5	137.26(15)
O6–Co1–O12	77.28(13)	O9–Co2–O12	106.17(13)
O6–Co1–N1	164.53(15)	O9–Co2–N4	88.81(15)
O6–Co1–N2	83.59(14)	O9–Co2–N5	108.69(16)
O12–Co1–N1	96.38(14)	O12–Co2–N4	164.82(15)
O12–Co1–N2	130.27(15)	O12–Co2–N5	83.36(14)
N1–Co1–N2	90.16(16)	N4–Co2–N5	89.58(16)
2			
Bond	Lengths	Bond	Lengths
Zn1–O1	1.931(3)	Zn2–O6	2.023(3)
Zn1–O6	2.055(3)	Zn2–O7	1.922(3)
Zn1–O12	2.019(3)	Zn2–O12	2.113(3)
Zn1–N1	2.097(4)	Zn2–N4	2.123(3)
Zn1–N2	2.096(3)	Zn2–N5	2.046(3)
Bond	Angles	Bond	Angles
O1–Zn1–O6	108.04(12)	O6–Zn2–O7	114.10(12)
O1–Zn1–O12	116.24(12)	O6–Zn2–O12	77.70(11)
O1–Zn1–N1	89.63(13)	O6–Zn2–N4	95.33(12)
O1–Zn1–N2	108.67(13)	O6–Zn2–N5	127.44(13)
O6–Zn1–O12	79.13(11)	O7–Zn2–O12	107.22(12)
O6–Zn1–N1	161.73(11)	O7–Zn2–N4	89.95(12)
O6–Zn1–N2	81.76(13)	O7–Zn2–N5	118.20(14)
O12–Zn1–N1	97.52(13)	O12–Zn2–N4	162.83(12)
O12–Zn1–N2	134.68(12)	O12–Zn2–N5	82.45(12)
N1–Zn1–N2	88.30(13)	N4–Zn2–N5	89.74(13)

crystal structure which is different from the structures of 1:1 [19, 22, 51], 2:3 [7, 30, 52], 2:4 [39], 3:3 [19, 22], 4:4 [19], 1:3 [53], 2:6 [54], 1:6 [55] and 1:7 [56] ($L:M^{2+}$) reported earlier. The molecular structures of complexes **1** and **2** are shown in Figs. 3a and S1a. In the coordination environment of Co2 and Zn1, two phenolic oxygen atoms (O9, O12 or O6, O12) and oxime nitrogen atoms (N4, N5 or N1, N2) are in the *cis* positions with each other (Figs. 3b and S1b). Due to the long distance between the two M^{II} atoms, there is no interaction between them.

In addition, the supramolecular structures of complexes **1** and **2** are similar. In the crystal structure of complex **1**, there are two groups of intramolecular hydrogen bonds and six groups of intermolecular hydrogen bonds; these intermolecular hydrogen bonding interactions form a 3D supramolecular structure, as shown in Table 4 and Fig. 4 [57, 58]. For the crystal structure of complex **2**, there are

Table 4 Hydrogen bonding interactions (Å, °) for **1** and **2**

D–H···A	d(D–H)	d(H···A)	d(D···A)	∠D–H···A	Symmetry Code
1					
O13–H13C···O5	0.84	2.45	3.278(8)	170	
C11–H11···O2	0.93	2.28	2.657(6)	104	
C12–H12A···O9	0.97	2.34	3.300(6)	172	$3/2-x, -1/2+y, z$
C19–H19···O13	0.93	2.49	3.381(8)	161	$1/2+x, y, 1/2-z$
C35–H35··O8	0.93	2.30	2.666(6)	103	
C38–H38··O7	0.93	2.43	3.320(7)	159	$-1/2+x, 1/2-y, 1-z$
C45–H45B··O7	0.97	2.53	3.119(7)	119	$-1+x, y, z$
C46–H46A··O10	0.96	2.57	3.255(7)	129	$3/2-x, 1/2+y, z$
2					
O13–H13C···O11	0.85	2.34	3.143(7)	158	
O13–H13C···O9	0.85	1.92	2.749(7)	166	$1/2+x, y, 1/2-z$
C11–H11···O2	0.93	2.30	2.669(6)	103	
C14–H14···O3	0.93	2.45	3.328(6)	158	$-1/2+x, 3/2-y, 1-z$
C23–H23A···O3	0.97	2.53	3.116(6)	119	$-1+x, y, z$
C35–H35···O8	0.93	2.25	2.645(5)	105	
C36–H36B···O1	0.97	2.36	3.325(5)	172	$3/2-x, 1/2+y, z$

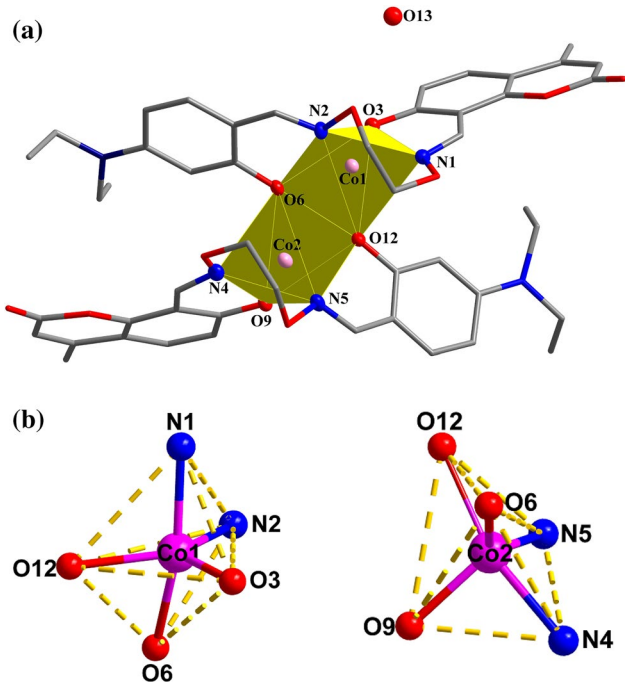

Fig. 3 **a** Molecular structure and atom numbering of **1** with 30% probability displacement ellipsoids (hydrogen atoms are omitted for clarity). **b** Coordination polyhedrons for Co^{II} ions

two sets of intramolecular hydrogen bonds and five sets of intermolecular hydrogen bonds as shown in Fig. S2 [59–61]. The 3D supramolecular structure of complex **2** is similar to complex **1**.

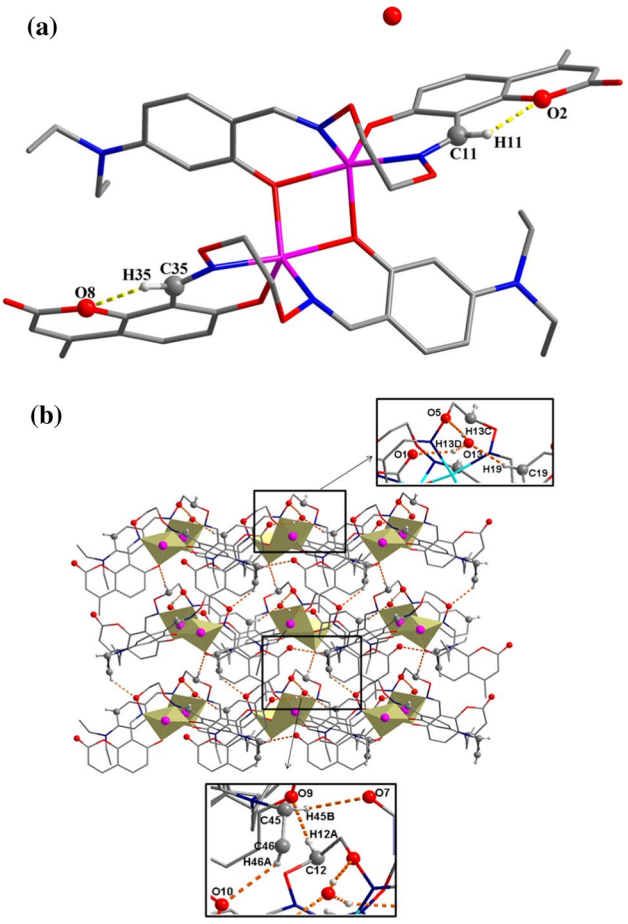

Fig. 4 **a** View of the intramolecular hydrogen bonds and **b** 3D supramolecular structure of complex **1**

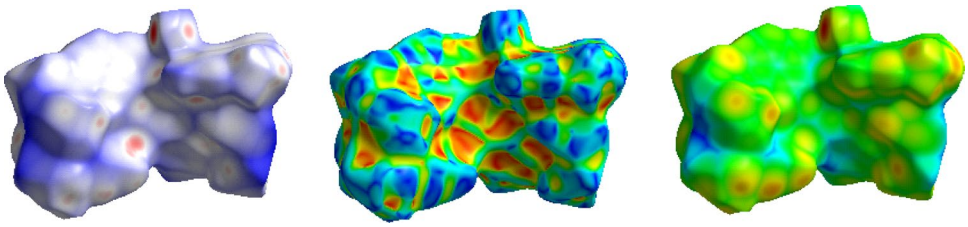

Fig. 5 Hirshfeld surfaces are mapped with d_{norm}, shape index and d_i of complex **1**

Hirshfeld surfaces analyses

The Hirshfeld surfaces [62–64] of complex **1** are mapped over (a) d_{norm}, (b) the shape index and (c) d_i in Fig. 5. As shown in Fig. 6, the 2D fingerprint chart shows different intermolecular interactions. In Fig. 5, Hirshfeld surface analysis was performed on complex **1** [65], which shows the surfaces mapped on d_{norm}, the shape index and d_i. The bright red area on the depression of Hirshfeld surface indicates the presence of O···H interactions in complex **1**, and light red spots indicate C–H···O interactions, while other raised blue areas indicate the presence of C···H, H···H and C···C interactions in complex **1**. The Hirshfeld surfaces mapped with d_{norm}, shape index and d_i of complex **2** are similar to those of complex **1** because the complexes **1** and **2** are isomorphic. Figure 6 shows the generated 2D fingerprints [66], corresponding to O···H, C···H and H···H interactions on the Hirshfeld surface of complexes **1** (a) and **2** (b), respectively. To provide context, the outline of the full fingerprint is shown in gray, and the blue area shows individual contact. For complexes **1** and **2**, the proportions of O•••H/H•••O, C•••H/H•••C and H•••H interactions in each molecule are similar to the total surface, while the differences in fingerprint plots of complexes **1** and **2** are caused by different geometrical parameters of disordered Et-groups in these two structures. Because of the existence of these hydrogen bonds, complexes **1** and **2** can be stabilized.

Fluorescence properties

The fluorescence spectra of H_2L and its complexes **1** and **2** were measured in ethanol (2.5×10^{-5} M) at room temperature, as shown in Fig. 7. At an excitation wavelength of 350 nm, the ligand H_2L has a broad absorption peak at approximate 431 nm, which is attributed to π–π^* intraligand transition [67]. Compared with the ligand H_2L, the absorption peak intensities of complexes **1** and **2** at 431 nm are significantly different. Compared with the ligand H_2L, the fluorescence intensity of complex **1** is significantly reduced, indicating that Co^{II} ions have fluorescence quenching properties. On the other hand, the fluorescence intensity of complex **2** was significantly enhanced due to the coordination of the ligand $(L)^{2-}$ units with Zn^{II} ions and enhanced the coplanarity of the conjugated system.

Conclusion

In this paper, two new dinuclear complexes were synthesized via H_2L and $Co(OAc)_2{\cdot}4H_2O$ and $Zn(OAc)_2{\cdot}H_2O$, respectively. A series of structural characterizations were performed for complexes **1** and **2**. The X-ray single-crystal structure determinations indicate that both Co^{II} and Zn^{II} atoms in complexes **1** and **2** are penta-coordinated. The coordination configurations of the two metal atoms in complexes **1** and **2** are different: one is a twisted trigonal bipyramid configuration, and the other is a twisted square pyramid configuration. The Hirshfeld surfaces and 3D fingerprints can explain the atom-to-pair contact of crystals, which can quantify the intermolecular interactions. In addition, the coordination of Co^{II} and Zn^{II} ions with the ligand $(L)^{2-}$ units results in fluorescence quenching and enhancement, respectively.

Supplementary material

Crystallographic data have been deposited with the Cambridge Crystallographic Data Centre as supplementary publication, CCDC Nos. 1975065 and 1975064 for complexes **1** and **2**, respectively. Copies of the data can be obtained free of charge on application to CCDC, 12 Union Road, Cambridge CB2 1EZ, UK (Telephone: +44-01223-762910; Fax: +44-1223-336033; E-mail: deposit@ccdc.cam.ac.uk). These data can be also obtained free of charge at www.ccdc.cam.ac.uk/conts/retrieving.html.

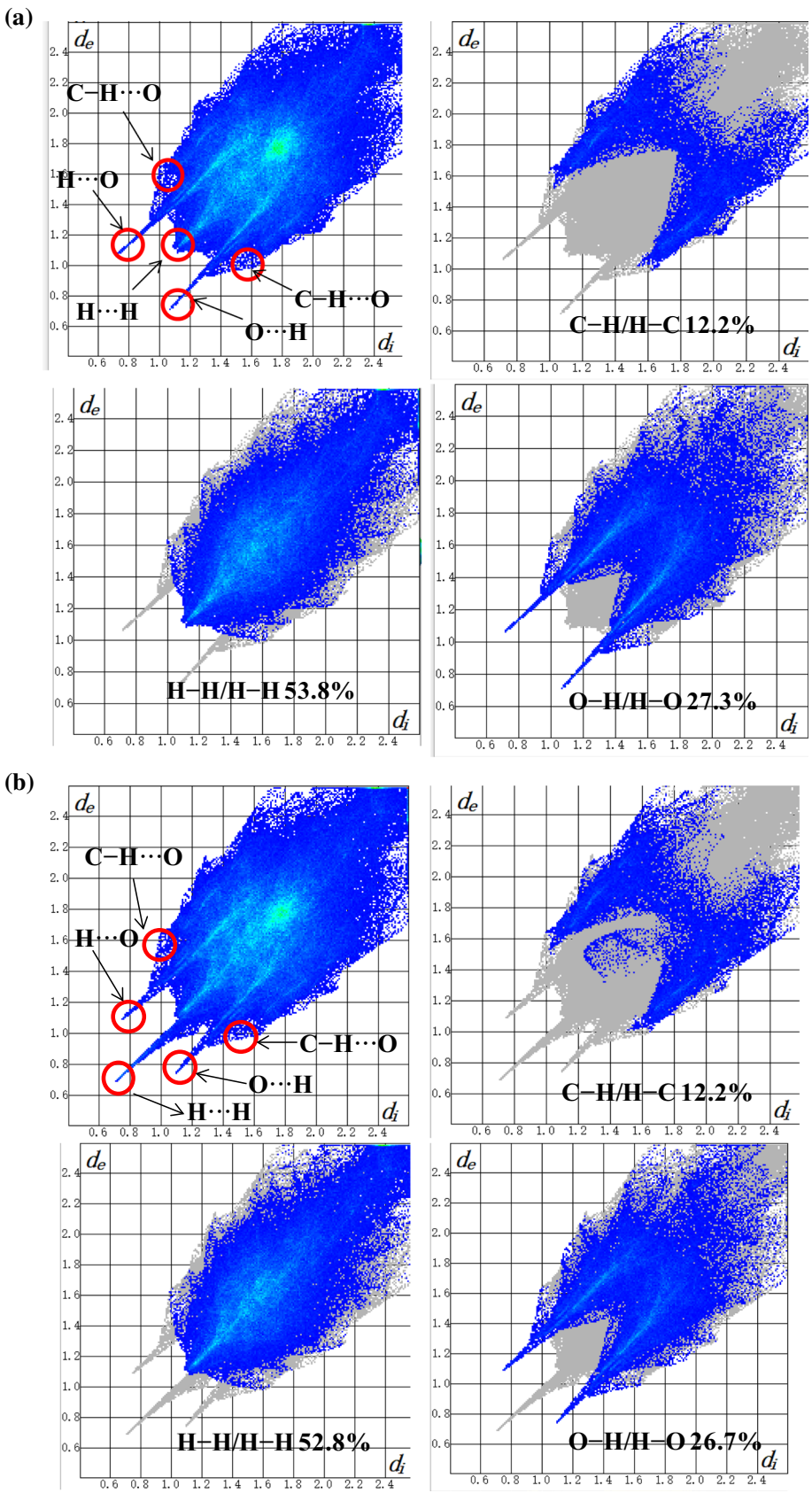

Fig. 6 Fingerprint plot of **1** and **b 2**: full and resolved into full and resolved into O···H, C···H and H···H contacts showing the percentages of contacts contributed to the total Hirshfeld area of molecule

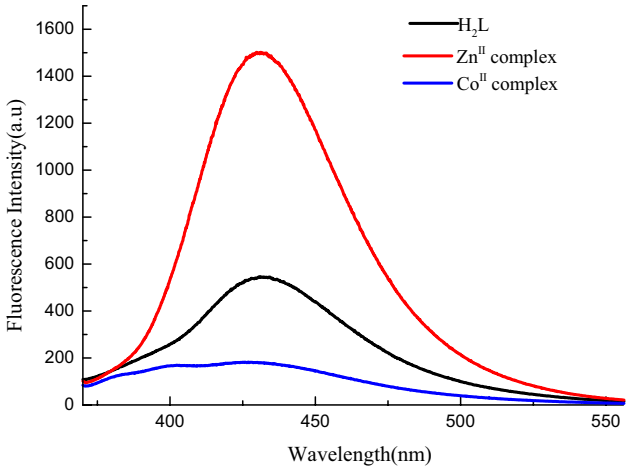

Fig. 7 Emission spectra of H_2L and its complexes **1** and **2**

Acknowledgements Fundings from the National Science Foundation (21761018) and the Program for Excellent Team of Scientific Research in Lanzhou Jiaotong University (201706) are gratefully acknowledged.

Compliance with ethical standards

Conflict of interest The authors declare no competing financial interests.

References

1. Chai LQ, Huang JJ, Zhang HS (2014) Spectrochim Acta A 131:526–530
2. Sun YX, Pan YQ, Xu X, Zhang Y (2019) Crystals 9:607
3. Song XQ, Peng YQ, Chen GQ, Wang XR, Liu PP (2015) Inorg Chim Acta 427:13–21
4. Li J, Zhang HJ, Chang J, Sun YX, Huang YQ (2018) Crystals 8:176
5. Liu PP, Sheng L, Song XQ, Xu WY, Liu YA (2015) Inorg Chim Acta 434:252–257
6. Jia HR, Chang J, Zhang HJ, Li J, Sun YX (2018) Crystals 8:272
7. Yu M, Mu HR, Liu LZ, Li N, Bai Y, Dong XY (2019) Chin J Inorg Chem 35:1109–1120
8. Chang J, Zhang HJ, Jia HR, Sun YX (2018) Chin J Inorg Chem 34:2097–2107
9. Dong XY, Zhao Q, Kang QP, Li XY, Dong WK (2018) Crystals 8:230
10. An XX, Zhao Q, Mu HR, Dong WK (2019) Crystals 9:101
11. Zhang LW, Zhang Y, Cui YF, Yu M, Dong WK (2020) Inorg Chim Acta 506:119534
12. Li XY, Kang QP, Liu C, Zhang Y, Dong WK (2019) New J Chem 43:4605–4619
13. Wang F, Liu LZ, Gao L, Dong WK (2018) Spectrochim Acta A 203:56–64
14. Zhang LW, Li XY, Kang QP, Liu LZ, Ma JC, Dong WK (2018) Crystals 8:173
15. Song XQ, Liu PP, Liu YA, Zhou JJ, Wang XL (2016) Dalton Trans 45:8154–8163
16. Zhang HJ, Chang J, Jia HR, Sun YX (2018) Chin J Inorg Chem 34:2261–2270
17. Petrick M, Florian B, Katja L, Guntram R, Réne P (2012) Molecules 17:7121–7150
18. Bella SD, Fragala I (2000) Synth Met 115:191–196
19. Kang QP, Li XY, Wang L, Zhang Y, Dong WK (2019) Appl Organomet Chem 33:e5013
20. Azam M, Al-Resayes SI, Trzesowska-Kruszynska A, Kruszynski R, Kuma P (2017) Polyhedron 124:177–183
21. Liu LZ, Wang L, Yu M, Zhao Q, Zhang Y, Sun YX, Dong WK (2019) Spectrochim Acta A 222:117209
22. Kang QP, Li XY, Wei ZL, Zhang Y, Dong WK (2019) Polyhedron 165:38–50
23. Gao L, Liu C, Wang F, Dong WK (2018) Crystals 8:77
24. Yamamura M, Takizawa H, Sakamoto N, Nabeshima T (2013) Tetrahedron Lett 54:7049–7052
25. Manna AK, Mondal J, Chandra R, Rout K, Patra GK (2018) Sens Actuators B 10:2317–2326
26. Pan YQ, Xu X, Zhang Y, Zhang Y, Dong WK (2020) Spectrochim Acta A 229:117917
27. Pushkarev AP, Balashova TV, Kukinov AA, Arsenyev MV, Yablonskiy AN, Kryzhkov DI, Andreev BA, Rumyantcev RV, Fukin GK, Bochkarev MN (2017) Dalton Trans 46:10408–10417
28. Zhao Q, An XX, Liu LZ, Dong WK (2019) Inorg Chim Acta 490:6–15
29. Liu LZ, Yu M, Li XY, Kang QP, Dong WK (2019) Chin J Inorg Chem 35:1283–1294
30. Zhang Y, Liu LZ, Peng YD, Li N, Dong WK (2019) Transit Met Chem 44:627–639
31. Wei ZL, Wang L, Wang JF, Guo WT, Zhang Y, Dong WK (2020) Spectrochim Acta A 228:117775
32. Hao J, Li XY, Zhang Y, Dong WK (2018) Materials 11:523
33. Pan YQ, Zhang Y, Yu M, Zhang Y, Wang L (2020) Appl Organomet Chem 34:e5441
34. Zhang LW, Liu LZ, Wang F, Dong WK (2018) Molecules 23:1141
35. Dong XY, Zhao Q, Wei ZL, Mu HR, Zhang H, Dong WK (2018) Molecules 23:1006
36. Ren ZL, Hao J, Hao P, Dong XY, Bai Y, Dong WK (2018) Z Naturforsch B 73:203–210
37. Liu C, An XX, Cui YF, Xie KF, Dong WK (2020) Appl Organomet Chem 34:e5272
38. Bartocci S, Sabaté F, Bosque R, Keymeulen F, Bartik K, Rodríguez L, Cort AD (2016) Dyes Pig 135:94–101
39. Shi YS, Li YH, Cui GH, Dong GY (2020) CrystEngComm 22:905–915
40. Yang YJ, Li YH, Liu D, Cui GH (2020) CrystEngComm 22:1166–1175
41. Xiao QQ, Dong GY, Li YH, Cui GH (2019) Inorg Chem 58:15696–15699
42. Wei XJ, Liu D, Li YH, Cui GH (2019) J Solid State Chem 272:138–147
43. Su Q, Zhao Q, An XX, Wang YB, Li XY, Dong WK (2019) Chin J Inorg Chem 35:524–536
44. Wu HL, Pan GL, Bai YC, Zhang YH, Wang H, Shi FR, Wang XL, Kong J (2014) J Photochem Photobiol B 135:33–43
45. Zhang Y, Yu M, Pan YQ, Zhang Y, Xu L, Dong XY (2020) Appl Organomet Chem 34:e5442
46. Sheldrick GM (2008) Acta Cryst A64:112–122
47. Sheldrick GM (2015) Acta Cryst C71:3–8
48. An XX, Liu C, Chen ZZ, Xie KF, Zhang Y (2019) Crystals 9:602
49. Dong XY, Kang QP, Li XY, Ma JC, Dong WK (2018) Crystals 8:139
50. Peng YD, Wang F, Gao L, Dong WK (2018) J Chin Chem Soc 65:893–899
51. Akine S, Nabeshima T (2009) J Chem Soc Dalton Trans 46:10377–10628
52. Akine S, Taniguchi T, Nabeshima T (2004) Inorg Chem 43:6142–6144

53. Akine S, Kagiyama S, Nabeshima T (2010) Inorg Chem 49:2141–2152
54. Akine S, Sunaga TS, Nabeshima T (2011) Chem Eur J 17:6853–6861
55. Akine S, Sunaga TS, Taniguchi T, Miyazaki H, Nabeshima T (2007) Inorg Chem 46:2959–2961
56. Yamamura M, Miyazaki H, Iida M, Akine S, Nabeshima T (2011) Inorg Chem 50:5315–5317
57. Kang QP, Li XY, Zhao Q, Ma JC, Dong WK (2018) Appl Organomet Chem 32:e4379
58. Dong WK, Zhu LC, Dong YJ, Ma JC, Zhang Y (2016) Polyhedron 117:148–154
59. Sun YX, Wang L, Dong XY, Ren ZL, Meng WS (2013) Synth React Inorg Met-Org Nano-Met Chem 43:599–603
60. Chai LQ, Liu G, Zhang YL, Huang JJ, Tong JF (2013) J Coord Chem 66:926–3938
61. Wu HL, Bai Y, Yuan JK, Wang H, Pan GL, Fan XY, Kong J (2012) J Coord Chem 65:2839–2851
62. Wu HL, Pan GL, Bai YC, Wang H, Kong J (2015) Res Chem Intermed 41:3375–3388
63. Spackman MA, McKinnon JJ, Jayatilaka D (2008) CrystEngComm 10:377–388
64. Spackman MA, Jayatilaka D (2009) CrystEngComm 11:19–32
65. McKinnon JJ, Spackman MA, Mitchell AS (2004) Acta Crystallogr B 60:627–668
66. Fabbiani FPA, Byrne LT, Mckinnon JJ, Spackman MA (2007) CrystEngComm 9:728–731
67. Parkin A, Barr G, Dong W, Gilmore CJ, Jayatilaka D, Mckinnon JJ, Spackman MA, Wilson CC (2007) CrystEngComm 9:648–652